Journal of Applied Physics

RESEARCH ARTICLE | JULY 07 2023

# Defect level in κ-$Ga_2O_3$ revealed by thermal admittance spectroscopy

Amanda Langørgen ; Ymir Kalmann Frodason ; Robert Karsthof ; Holger von Wenckstern ; Ingvild Julie Thue Jensen ; Lasse Vines ; Marius Grundmann

*J. Appl. Phys.* 134, 015701 (2023)
https://doi.org/10.1063/5.0150994

View Online
Export Citation
CrossMark

20 February 2024 10:56:07

Journal of Applied Physics | ARTICLE | pubs.aip.org/aip/jap

# Defect level in $\kappa$-$Ga_2O_3$ revealed by thermal admittance spectroscopy

Cite as: J. Appl. Phys. **134**, 015701 (2023); doi: 10.1063/5.0150994
Submitted: 17 March 2023 · Accepted: 14 June 2023 ·
Published Online: 7 July 2023

Amanda Langørgen,[1,a)] Ymir Kalmann Frodason,[1] Robert Karsthof,[1] Holger von Wenckstern,[1,2] Ingvild Julie Thue Jensen,[1,3] Lasse Vines,[1] and Marius Grundmann[2]

## AFFILIATIONS

[1]Department of Physics/Centre for Materials Science and Nanotechnology, University of Oslo, P.O. Box 1048, Blindern, Oslo N-0316, Norway
[2]Universität Leipzig, Fakultät für Physik und Geowissenschaften, Felix-Bloch-Institut, D-04103 Leipzig, Germany
[3]SINTEF, Forskningsveien 1, 0373 Oslo, Norway

[a)]**Author to whom correspondence should be addressed:** amandl@uio.no

## ABSTRACT

Defects in pulsed-laser deposition grown $\kappa$-$Ga_2O_3$ have been investigated using thermal admittance spectroscopy and secondary ion mass spectrometry (SIMS). A $\kappa$-$Ga_2O_3$ film was grown on either a tin-doped indium oxide or an aluminum-doped zinc oxide buffer layer on a sapphire substrate functioning as back contact layer in vertical diode structures. In both sample types, a distinct signature in the capacitance signal was observed in the temperature range of 150–260 K. The corresponding defect charge-state transition level, labeled $E_0$, was found to exhibit an activation energy of 0.21 eV. Potential candidates for the $E_0$ level were investigated using a combination of SIMS and hybrid-functional calculations. SIMS revealed the main impurities in the sample to be tin, silicon, and iron. The hybrid-functional calculations predict the acceptor levels of substitutional iron to lie 0.7–1.2 eV below the conduction band minimum depending on Ga-site, making $Fe_{Ga}$ an unlikely candidate for the $E_0$ level. Furthermore, Si as well as Sn substituting on the sixfold coordinated Ga2 site and the fivefold coordinated Ga3 and Ga4 sites are all shallow donors in $\kappa$-$Ga_2O_3$, similar to that of $\beta$-$Ga_2O_3$. Sn substituting on the fourfold Ga1 site is, however, predicted to have levels in the bandgap at 0.15 and 0.24 eV below the conduction band minimum, in accordance with the extracted activation energy for $E_0$. Thus, we tentatively assign $Sn_{Ga1}$ as the origin of the $E_0$ level.

*Published under an exclusive license by AIP Publishing.* https://doi.org/10.1063/5.0150994

20 February 2024 10:56:07

## I. INTRODUCTION

Gallium sesquioxide is a semiconductor material that has seen a rapid surge of interest in recent years and a correspondingly fast technological advancement. Properties, such as an ultrawide bandgap of around 5 eV,[1] a large critical field strength,[2] and a widely tunable *n*-type conductivity, make the material promising for high-power electronic devices and ultraviolet optoelectronics.[3] Five different polymorphs of the material are usually reported.[4] To date, the main focus has been directed toward the thermodynamically stable monoclinic phase, $\beta$-$Ga_2O_3$. However, there is a growing interest in the metastable phases of the material, among which the orthorhombic phase, $\kappa$-$Ga_2O_3$, is considered the second most stable polymorph, with a thermal stability up to around 700 °C.[5–11] $\kappa$-$Ga_2O_3$ has been calculated to have a large spontaneous polarization of $23\,\mu C\,cm^{-2}$, which makes the material intriguing for devices based on polarization doping including high-electron mobility transistors.[5,12,13]

In order to accomplish functioning and reliable devices from $\kappa$-$Ga_2O_3$, an understanding and control of electrically active defects is imperative. To date, however, both the experimental and theoretical knowledge of defects in the material is scarce. The experimental investigations have been impeded in part due to the limitations in growing a high-quality material with a controlled conductivity. Only recently, for instance, the growth of $\kappa$-$Ga_2O_3$ without any rotational domains was realized,[14] as well as the first report on Schottky barrier diodes and pn-heterojunctions.[15] Well-behaved rectifying junctions are a prerequisite for performing several defect spectroscopy techniques, such as deep-level transient spectroscopy (DLTS) and thermal admittance spectroscopy (TAS). As of now, there exists one study where DLTS and TAS measurements have been conducted on $\kappa$-$Ga_2O_3$, in which they study


Published under an exclusive license by AIP Publishing

$\kappa$-films grown by halide vapor phase epitaxy on GaN/sapphire templates.[16] The measurements reveal the presence of several deep levels with trap energies ranging from 0.3 to 1 eV below the conduction band minimum (CBM).

In this work, we study $\kappa$-$Ga_2O_3$ grown by pulsed-laser deposition (PLD) on two different substrates, aluminum-doped zinc oxide and tin-doped indium oxide, functioning as back contacts of vertical Schottky barrier diodes. We use a stack of $PtO_x$/Pt as Schottky contacts. Current–voltage measurements confirm rectifying diodes. From capacitance–voltage measurements, we extract an effective carrier concentration in the low $10^{18}$ $cm^{-3}$ range. TAS reveals a defect level with an activation energy of about 0.21 eV for a thermal emission to the CBM. Combining secondary ion mass spectrometry (SIMS) data and hybrid-functional calculations leads us to propose Sn substituting on the tetrahedrally coordinated Ga-position as a possible origin for this observed defect level.

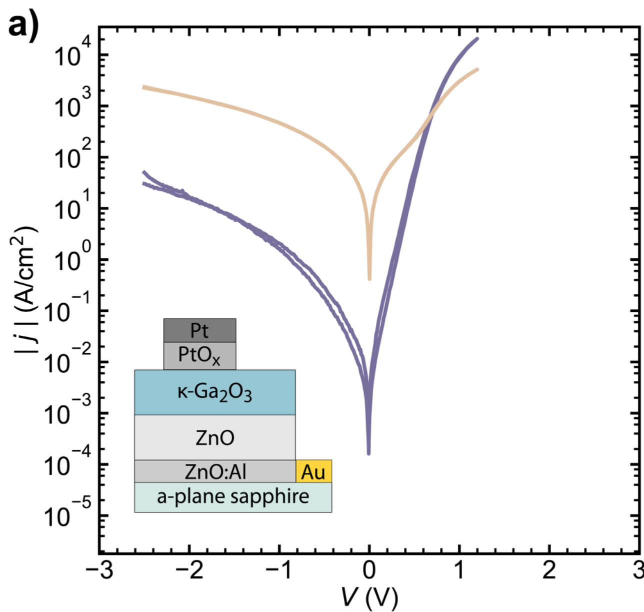


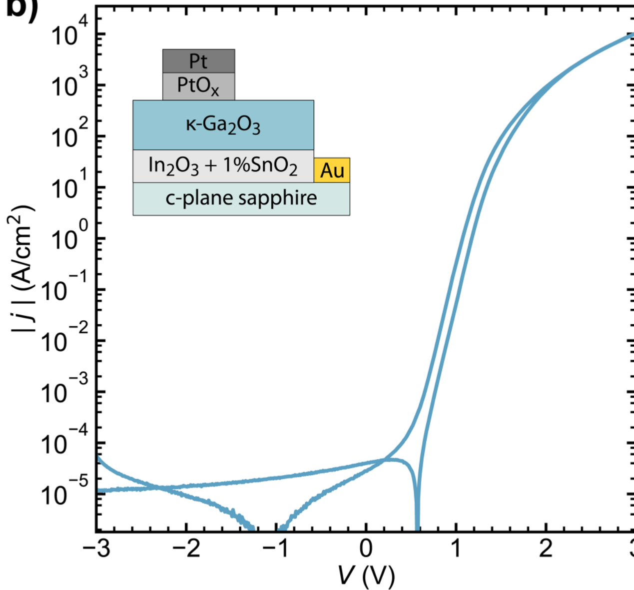


**FIG. 1.** *j-V* characteristics for two different diode structures. The structures are depicted schematically in the plots. (a) The two *j-V* curves show the least and the most rectifying diode on the AZO-sample. (b) A representative *j-V* curve for the diode structure with an ITO-substrate functioning as the back contact layer.

## II. METHODS

The $\kappa$-$Ga_2O_3$ samples used in this study were grown by PLD (around 620 °C growth temperature) on either a stack of nominally undoped ZnO on a highly conductive Al-doped ZnO (AZO) back contact layer or on a $In_2O_3$ layer with 2 at. % $SnO_2$ (ITO). In both cases, the substrate was single-side polished $10 \times 10\,mm^2$ sapphire substrates, with a-plane orientation in the first case and c-plane in the latter (see Ref. 15 for more details of the sample growth). The resulting thickness of the $\kappa$-$Ga_2O_3$ layer is 25–400 nm. The AZO-sample was subsequently cut into a $5 \times 5\,mm^2$ sample using a laser cutter.

For electrical characterization, circular Schottky contacts with diameters between 150 and 750 $\mu$m were deposited using reactive DC sputtering. $PtO_x$ was deposited in 50 SCCM $O_2$/50 SCCM Ar with a sputtering power of 30 W. Metallic Pt was subsequently DC sputtered in an Ar atmosphere. The $\kappa$-$Ga_2O_3$-film does not fully cover the substrate stack but leaves the corners exposed. Hence, by depositing Au in the corners, it is possible to make an ohmic contact with the conducting AZO or ITO layer underneath. Layouts of the diode structures are depicted in Figs. 1(a) and 1(b).

Current–voltage ($I$–$V$) and capacitance–voltage ($C$–$V$) measurements of the diodes were performed at room temperature. The $I$–$V$ characterization was carried out using an AGILENT 4155C semiconductor parameter analyzer connected to a SÜSS wafer prober system with tungsten needles, while the $C$–$V$ measurements were performed using a Boonton 7200 capacitance meter and a 1 MHz probing frequency.

TAS in the temperature range of 20–300 K was conducted using an Agilent 4280A LCR meter, with a 50 mV AC probing signal with nine measurement frequencies between 1 kHz and 1 MHz and a reverse bias of −0.5 V.

To identify and quantify impurities in the samples, SIMS was performed. A spectrometer of type Cameca IMS7f with a primary ion source of $O_2^-$ was employed for SIMS measurements. To measure the created crater depth, a Veeco Dektak 8 stylus profilometer was used. Implanted reference samples were used to convert counts into concentration.

First-principles calculations were performed using the projector augmented wave method[17,18] and the screened hybrid functional of Heyd, Scuseria, and Ernzerhof (HSE),[19] as implemented in the VASP code.[20] The Ga 3$d$ electrons were treated explicitly as valence electrons. The fraction of screened Hartree-Fock exchange was adjusted to $\alpha = 0.33$, as this parametrization reproduces the experimental direct bandgap value of 4.9 eV for $\beta$-$Ga_2O_3$.[1] For

20 February 2024 10:56:07


Published under an exclusive license by AIP Publishing

$\kappa$-$Ga_2O_3$, we obtain a comparable direct bandgap value of 5.0 eV, in line with previous HSE calculations by Gake *et al.*[21] The calculated lattice parameters ($a = 5.03$ Å, $b = 8.65$ Å, and $c = 9.27$ Å) are in good agreement with experimental data.[6]

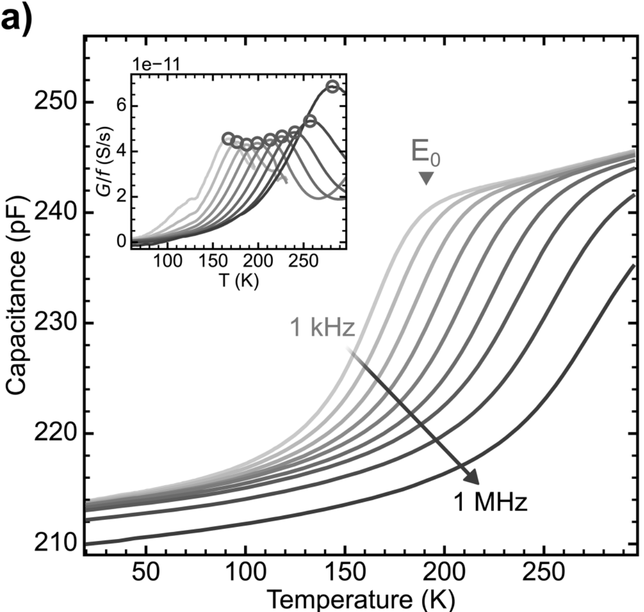


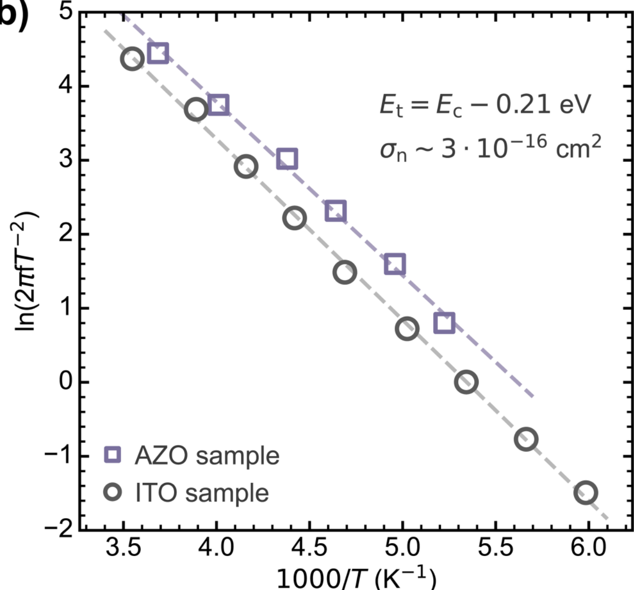


**FIG. 2.** Thermal admittance spectroscopy results. (a) Capacitance as a function of temperature for measurement frequencies from 1 kHz to 1 MHz for the $\kappa$-$Ga_2O_3$ grown on an ITO substrate. The inset shows the associated conductance measurement for the same frequencies. Offsets in conductance between the measurements have been removed for clarity. (b) Fits to the Arrhenius relation, and the extracted and calculated values for the trap energy level and capture cross section for both ITO- and AZO-substrate samples.

Defect formation energies and thermodynamic charge-state transition levels were evaluated using the formalism described in Ref. 22. The chemical potential of Sn, Si, and Fe impurities is referenced to the solubility-limiting phases $SnO_2$ (Sn), $SiO_2$ ($SiO_2$), and $Fe_2O_3$ (Fe), respectively, in the O-rich (Ga-rich) limit. Formation energies are plotted for intermediate conditions, which is taken to mean halfway between the O-rich and Ga-rich limit. For charged defects, we apply finite-size corrections following the scheme outlined in Refs. 23–25 with a static dielectric tensor $\varepsilon_{xx} = 17.0$, $\varepsilon_{yy} = 16.0$, and $\varepsilon_{zz} = 18.1$, calculated as described by Gake *et al.*,[21] but using the strongly constrained and appropriately normed (SCAN)[26] semilocal functional for the ionic contribution. Defect calculations were performed using 80-atom supercells ($2 \times 1 \times 1$ repetition of the conventional unit cell), a plane-wave cutoff of 400 eV, and a single special $k$-point at (0.25,0.25,0.25). Convergence tests for $Sn_{Ga}$ and $Fe_{Ga}$ employing a semilocal functional result in differences of about 0.1 eV between defect formation energies calculated using 80- and 480-atom supercells.

We use the same naming convention for different Ga- and O-sites as in Gake *et al.*[21]

## III. RESULTS AND DISCUSSION

### A. Current–voltage and capacitance–voltage

Typical current density–voltage ($j$–$V$) characteristics are shown in Fig. 1. The figure reveals a rectification between forward and reverse bias for both of the diode structures. The two $j$–$V$ curves in Fig. 1(a) show the most and the least rectifying diode on the AZO-substrate sample, which varies from above three orders of magnitude to roughly one order of magnitude. The $j$–$V$ characteristics of $\kappa$-$Ga_2O_3$ grown on an ITO-substrate, Fig. 1(b), show on average better diode behavior, displaying rectifications up to roughly eight orders of magnitude.[27] For both sample structures, the $j$–$V$ measurements confirm diode behavior required for capacitance spectroscopy measurements. Note that the hysteresis seen in the $j$–$V$ curve in Fig. 1(b) have been reported previously[15] and are related to the measurement time constant and charging currents.[28]

From $C$–$V$ measurements (not shown), we extract the net doping density ($N_D - N_A$) of the samples. For the $\kappa$-$Ga_2O_3$ layer grown on ITO, a net doping density between $2 \times 10^{18}$ cm$^{-1}$ and $5 \times 10^{18}$ cm$^{-3}$ was estimated using the calculated dielectric constant of ∼17. The Fermi level is, accordingly, close to CBM. For the AZO-substrate sample, the $C$–$V$ measurements reveal markedly larger variations in the net doping density between the diodes, varying from $2 \times 10^{17}$ cm$^{-3}$ to $4 \times 10^{18}$ cm$^{-3}$, suggesting an apparent lateral inhomogeneity. One possible explanation for this variation could be a capacitance contribution from the back surface interface between the $\kappa$-$Ga_2O_3$ and the ZnO layer,[15] effectively resulting in two bias-dependent capacitances connected in series giving rise to the observed large variability. In this case, the less varied net doping density values for the ITO sample could be explained by a better ohmic back contact.

20 February 2024 10:56:07

### B. Thermal admittance spectroscopy

Figure 2(a) shows TAS results for the ITO-substrate sample, where the measured capacitance as a function of temperature for



Published under an exclusive license by AIP Publishing

different probing frequencies reveal one capacitance step, interpreted as a charge-state transition level labeled $E_0$. The capacitance signal confirms that the free charge carriers arise in the $\kappa$-$Ga_2O_3$ layer, in accordance with the $C$–$V$-measurements, but that not all the carriers respond to a 1 MHz signal at room temperature. This frequency dependence may contribute to some of the variations observed in the extracted net doping density, as discussed above. The inset in Fig. 2(a) shows the corresponding probing frequency normalized conductance measurement. Note that the frequency normalized conductance displayed an offset between the measurement frequencies, which has been normalized for clarity. Importantly, the conductance characteristics also display the signature of a charge-state transition level $E_0$. Figure 2(b) shows the associated Arrhenius plot, which is constructed from the peak maxima in conductance. The activation energy for the trap ($E_c - E_t$) is found from the slope of the Arrhenius line to be 0.21 eV. The capture cross section was calculated to be approximately $3 \times 10^{-16}$ cm$^2$, using a theoretical value for the electron effective mass in $\kappa$-$Ga_2O_3$ of $0.26m_e$.[21] The same TAS-signature was observed in the AZO-substrate sample, and the corresponding Arrhenius plot for this diode structure is also shown in Fig. 2(b), which supports the assumption that $E_0$ is, indeed, a trap level in the $\kappa$-$Ga_2O_3$ films.

From the height of the capacitance step in Fig. 2(a), we find that the concentration of $E_0$ is roughly 12% of the room temperature net doping density. For the specific diode measured in Fig. 2(a), this amounts to a defect concentration of about $3 \times 10^{17}$ cm$^{-3}$. We similarly find for the AZO-substrate sample that the capacitance step in the TAS-measurement amounts to a defect concentration of 12% of the net doping density. The large spread in extracted $N_D$ values for the AZO-substrate sample, however, makes it necessary to exercise caution in deriving absolute concentrations based on $N_D$ for that sample.

Notably, we do not observe a freeze-out level in TAS measurements despite reaching temperatures down to 20 K. The remaining capacitance can at least partially be explained by the capacitance caused by the highly degenerate buffer layer. This capacitance contribution from the vertical structure makes the estimated concentration of $E_0$ of about $3 \times 10^{17}$ cm$^{-3}$, a lower bound.

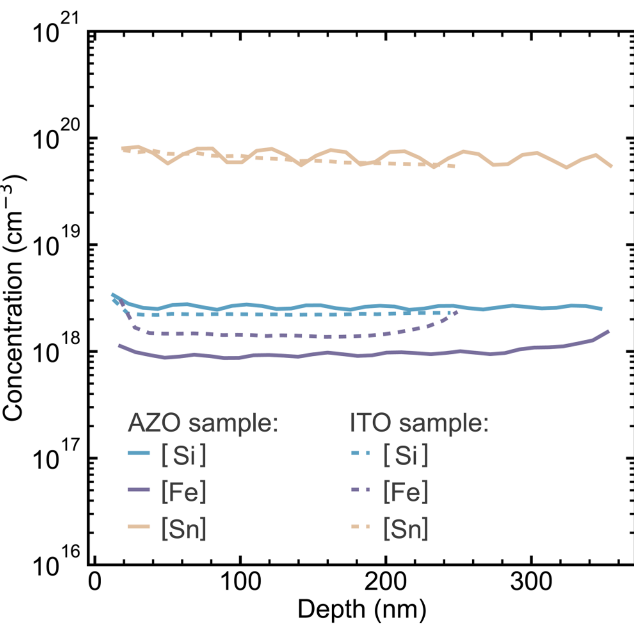


FIG. 3. Secondary ion mass spectrometry results for impurities Si, Fe, and Sn in both sample types.

### C. Secondary ion mass spectrometry

From SIMS measurements, we found Sn to be the most prevalent impurity in both sample types, with average concentrations of around $6 \times 10^{19}$ cm$^{-3}$ throughout the films, see Fig. 3. A considerable concentration of Sn is expected in the samples, as Sn is a prerequisite in the growth process and the $Ga_2O_3$ PLD targets used contain 2 at. % $SnO_2$.

The second most dominant impurity we find is Si, which in both sample types is found in concentrations of around $2 \times 10^{18}$ cm$^{-3}$. Si and Sn are the two most common donor dopants in $\beta$-$Ga_2O_3$, and a similar behavior is expected in $\kappa$-$Ga_2O_3$. The high values of $N_D$ can, therefore, be explained by the large concentrations of Si and Sn. Of note, however, is the difference between the acquired SIMS concentrations and $N_D$, where, e.g., the tin concentration is one order of magnitude larger than the typical $N_D$ values. This implies that (1) a large part of Sn in the crystal is not electrically active, or that (2) there is a substantial concentration of compensating acceptors present. However, we can at present not determine the dominant mechanism due to the lack of reliable mobility measurements.

Finally, we also find a considerable amount—$1 \times 10^{18}$ cm$^{-3}$—of Fe in the samples.

### D. Results of first-principles calculations

Hybrid functional calculations were performed to investigate possible candidates for the trap level observed in TAS, assuming an impurity-related origin. Guided by the findings from SIMS measurements, we have explored defects related to impurities Si, Sn, and Fe. It should be noted that at this point we cannot dismiss that the origin of the $E_0$ level could be related to intrinsic defects or a common impurity such as hydrogen (H) (the concentration of H was below the detection limit for our SIMS instrument of $\lesssim 1 \times 10^{18}$ cm$^{-3}$). However, assuming that the intrinsic defect structure is similar across different polymorphs,[21] we do not expect any intrinsic thermally stable shallow defects at concentrations compatible with $E_0$.[29–33]

In $n$-type material, both Si and Sn have the lowest formation energy when substituting for Ga compared to substituting for O or as interstitials. Based on previous theoretical studies on these impurities in $\beta$-$Ga_2O_3$[32,34] and $AlGaO_3$ alloys,[35] $Si_{Ga}$ and $Sn_{Ga}$ in $\kappa$-$Ga_2O_3$ are expected to either behave as shallow donors or $DX$-centers with a $\varepsilon(+/-)$ level in the bandgap. For Si, only the single positive charge state could be stabilized for all four Ga sites. It, therefore, seems like, akin to in $\beta$-$Ga_2O_3$,[35] Si is an efficient $n$-type dopant. From the lack of compatible charge-state transition

20 February 2024 10:56:07


Published under an exclusive license by AIP Publishing

levels in the band gap, Si is consequently not likely to give rise to the $E_0$ level.

In Fig. 4, the calculated formation energies for Ga-substitutional Sn in $\kappa$-$Ga_2O_3$ are shown. Sn substitution on the sixfold coordinated Ga2 position and on fivefold coordinated Ga3 and Ga4 positions exhibits $\varepsilon(+/-)$ levels inside the CB and will, thus, behave as shallow donors. Sn substituting for the fourfold coordinated Ga1, however, displays a different behavior with $\varepsilon(+/0)$ and $\varepsilon(0/-)$ levels inside the calculated bandgap at Fermi level values of $E_c - 0.24$ eV and $E_c - 0.15$ eV.

From the energy of the calculated charge-state transition levels, $Sn_{Ga1}$ appears as a possible candidate for the measured trap signature. Indeed, the energies of both $\varepsilon(+/0)$ and $\varepsilon(0/-)$ are close to the activation energy extracted from TAS measurements of 0.21 eV. Experimentally, we only observe one level. One explanation could be a difference in capture cross sections, possibly requiring higher temperatures or lower frequencies in order to observe both transitions for $Sn_{Ga1}$. On the other hand, the calculations are performed with an 80-atom supercell, which might not provide sufficiently converged results to distinguish whether $Sn_{Ga1}$ in fact exhibits positive-$U$ behavior or negative-$U$ like the three other Sn-configurations, as the two calculated charge-state transition levels are separated by merely 0.1 eV.

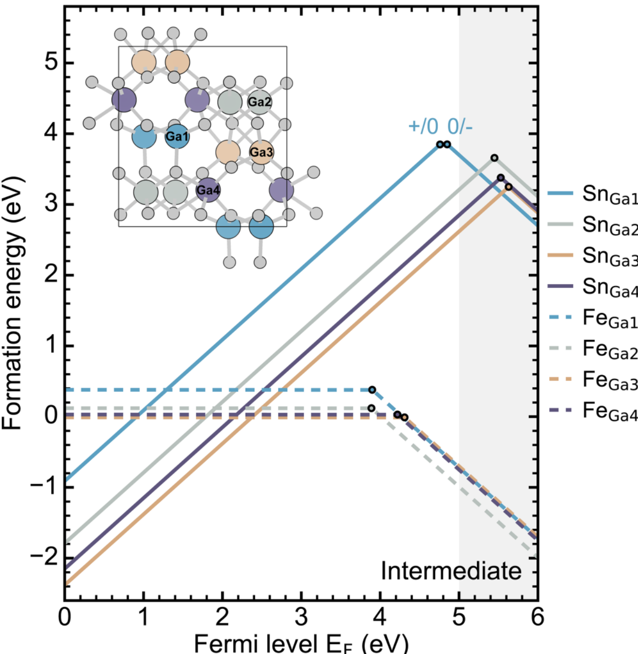


**FIG. 4.** Calculated formation energies for substitutional Sn and Fe on four inequivalent Ga-sites under intermediate conditions. The different Ga-sites are marked in the structure shown. The formation energies for the O-rich (Ga-rich) limit can be found by adding (subtracting) 1 eV. Our calculations result in a bandgap energy of 5 eV, and the shaded gray area represents Fermi-level energies that fall within the conduction band.

The experimental estimate for the defect concentration of $E_0$ is, however, hard to reconcile with what one would expect from the predicted stability of $Sn_{Ga1}$. The formation energy of $Sn_{Ga1}$ is 1.2 eV higher than the lowest energy configuration $Sn_{Ga4}$ for the +1 charge state. In an equilibrium situation, the concentration of $Sn_{Ga1}$ compared to other three configurations should, thus, be negligible, even at growth temperature.[15] On the other hand, depending on the growth conditions, the concentration ratios might not fully match up with an equilibrium case, and one could speculate that a portion of the Sn is frozen in on the tetrahedral position during growth. Indeed, in previous experimental studies on $\beta$-$Ga_2O_3$, one has observed that Si and Sn also occupy thermodynamically unfavored positions in the lattice.[36]

Similar to Si and Sn, Fe also prefers the Ga sites under $n$-type conditions, and calculated formation energies for substitutional Fe on four inequivalent Ga-positions are presented in Fig. 4. $Fe_{Ga}$ is predicted to act as a deep single acceptor, similar to that in $\beta$-$Ga_2O_3$. In $\beta$-$Ga_2O_3$, the transitions for Ga-substitutional Fe have been assigned to the $E_2$ level ($E_c - E_t \sim 0.78$ eV), which is commonly observed by DLTS.[37–42] From Fig. 4, we see that comparable transitions for substitutional Fe on fourfold and sixfold coordinated Ga-sites in $\kappa$-$Ga_2O_3$ are predicted to be somewhat deeper than in $\beta$-$Ga_2O_3$.

All the Fe transitions are relatively deep and correspondingly poor candidates for $E_0$. However, there is considerable uncertainty tied to the bandgap value, with reported values between 4.4 and 5.0 eV,[7,9,43–47] and, thus, the positions of the calculated transition levels relative to the CBM. With this uncertainty in mind, the apparently too deep transitions of $Fe_{Ga3}$ and $Fe_{Ga4}$ cannot be fully ruled out as being responsible for the observed TAS-signature.

20 February 2024 10:56:07

## E. Conclusion

In summary, we investigate a defect signature, $E_0$, in PLD-grown $\kappa$-$Ga_2O_3$ using a combination of TAS, SIMS, and hybrid-functional calculations. Two different vertical Schottky barrier diode types have been measured, one with AZO and the other with ITO functioning as the back contact. We use a stack of $PtO_x$/Pt as Schottky contacts. The $E_0$ level, with an activation energy of $\sim 0.21$ eV, is observed in TAS measurements on both diode types. Using SIMS, we identified Sn, Si, and Fe as dominant impurities in the $\kappa$-$Ga_2O_3$ films. Guided by the SIMS results, we performed hybrid-functional calculations, and we find $Sn_{Ga1}$ to have charge-state transition levels close to the measured activation energy for $E_0$.

## ACKNOWLEDGMENTS

Financial support was acknowledged from the Research Council of Norway through the GO2DEVICE project (Project No. 301740), the GO-POW project (Project No. 314017), and the Norwegian Micro- and Nano-Fabrication Facility (NorFab, Project No. 295864). This work was partially performed in the framework of GraFOx, a Leibniz-Science Campus, and partially funded by the Leibniz Association. Computations were performed on resources provided by UNINETT Sigma2—the National Infrastructure for High Performance Computing and Data Storage in Norway.


Published under an exclusive license by AIP Publishing

## AUTHOR DECLARATIONS

### Conflict of Interest

The authors have no conflicts to disclose.

### Author Contributions

**Amanda Langørgen:** Conceptualization (equal); Data curation (equal); Formal analysis (equal); Investigation (equal); Methodology (equal); Visualization (equal); Writing – original draft (lead); Writing – review & editing (equal). **Ymir Kalmann Frodason:** Conceptualization (equal); Data curation (equal); Formal analysis (equal); Funding acquisition (equal); Investigation (equal); Methodology (equal); Supervision (equal); Validation (equal); Writing – original draft (supporting); Writing – review & editing (equal). **Robert Karsthof:** Conceptualization (equal); Data curation (equal); Investigation (supporting); Methodology (equal); Supervision (equal). **Holger von Wenckstern:** Investigation (equal); Supervision (equal); Validation (equal); Writing – review & editing (equal). **Ingvild Julie Thue Jensen:** Funding acquisition (equal); Project administration (equal); Supervision (equal); Writing – review & editing (equal). **Lasse Vines:** Conceptualization (equal); Data curation (equal); Formal analysis (equal); Funding acquisition (equal); Investigation (equal); Methodology (equal); Project administration (equal); Supervision (equal); Validation (equal); Writing – review & editing (equal). **Marius Grundmann:** Funding acquisition (equal); Supervision (equal).

## DATA AVAILABILITY

The data that support the findings of this study are available from the corresponding author upon reasonable request.

## REFERENCES

[1]C. Janowitz, V. Scherer, M. Mohamed, A. Krapf, H. Dwelk, R. Manzke, Z. Galazka, R. Uecker, K. Irmscher, R. Fornari, M. Michling, D. Schmeißer, J. R. Weber, J. B. Varley, and C. G. V. de Walle, New J. Phys. **13**, 085014 (2011).
[2]J. D. Blevins, K. Stevens, A. Lindsey, G. Foundos, and L. Sande, IEEE Trans. Semicond. Manuf. **32**, 466 (2019).
[3]A. J. Green, J. Speck, G. Xing, P. Moens, F. Allerstam, K. Gumaelius, T. Neyer, A. Arias-Purdue, V. Mehrotra, A. Kuramata, K. Sasaki, S. Watanabe, K. Koshi, J. Blevins, O. Bierwagen, S. Krishnamoorthy, K. Leedy, A. R. Arehart, A. T. Neal, S. Mou, S. A. Ringel, A. Kumar, A. Sharma, K. Ghosh, U. Singisetti, W. Li, K. Chabak, K. Liddy, A. Islam, S. Rajan, S. Graham, S. Choi, Z. Cheng, and M. Higashiwaki, APL Mater. **10**, 029201 (2022).
[4]M. Bosi, P. Mazzolini, L. Seravalli, and R. Fornari, J. Mater. Chem. C **8**, 10975 (2020).
[5]M. B. Maccioni and V. Fiorentini, Appl. Phys. Express **9**, 041102 (2016).
[6]I. Cora, F. Mezzadri, F. Boschi, M. Bosi, M. Čaplovičová, G. Calestani, I. Dódony, B. Pécz, and R. Fornari, CrystEngComm **19**, 1509 (2017).
[7]M. Pavesi, F. Fabbri, F. Boschi, G. Piacentini, A. Baraldi, M. Bosi, E. Gombia, A. Parisini, and R. Fornari, Mater. Chem. Phys. **205**, 502 (2018).
[8]X. Xia, Y. Chen, Q. Feng, H. Liang, P. Tao, M. Xu, and G. Du, Appl. Phys. Lett. **108**, 202103 (2016).
[9]Y. Oshima, E. G. Víllora, Y. Matsushita, S. Yamamoto, and K. Shimamura, J. Appl. Phys. **118**, 085301 (2015).
[10]R. Fornari, M. Pavesi, V. Montedoro, D. Klimm, F. Mezzadri, I. Cora, B. Pécz, F. Boschi, A. Parisini, A. Baraldi, C. Ferrari, E. Gombia, and M. Bosi, Acta Mater. **140**, 411 (2017).
[11]Y. Yao, S. Okur, L. A. M. Lyle, G. S. Tompa, T. Salagaj, N. Sbrockey, R. F. Davis, and L. M. Porter, Mater. Res. Lett. **6**, 268 (2018).
[12]S. B. Cho and R. Mishra, Appl. Phys. Lett. **112**, 162101 (2018).
[13]K. Shimada, Mater. Res. Express **5**, 036502 (2018).
[14]H. Nishinaka, O. Ueda, D. Tahara, Y. Ito, N. Ikenaga, N. Hasuike, and M. Yoshimoto, ACS Omega **5**, 29585 (2020).
[15]M. Kneiß, D. Splith, P. Schlupp, A. Hassa, H. von Wenckstern, M. Lorenz, and M. Grundmann, J. Appl. Phys. **130**, 084502 (2021).
[16]A. Y. Polyakov, V. I. Nikolaev, A. I. Pechnikov, S. I. Stepanov, E. B. Yakimov, M. P. Scheglov, I. V. Shchemerov, A. A. Vasilev, A. A. Kochkova, A. V. Chernykh, A. V. Chikiryaka, and S. J. Pearton, APL Mater. **10**, 061102 (2022).
[17]P. E. Blöchl, Phys. Rev. B **50**, 17953 (1994).
[18]G. Kresse and D. Joubert, Phys. Rev. B **59**, 1758 (1999).
[19]A. V. Krukau, O. A. Vydrov, A. F. Izmaylov, and G. E. Scuseria, J. Chem. Phys. **125**, 224106 (2006).
[20]G. Kresse and J. Furthmüller, Phys. Rev. B **54**, 11169 (1996).
[21]T. Gake, Y. Kumagai, and F. Oba, Phys. Rev. Mater. **3**, 044603 (2019).
[22]C. Freysoldt, B. Grabowski, T. Hickel, J. Neugebauer, G. Kresse, A. Janotti, and C. G. V. de Walle, Rev. Mod. Phys. **86**, 253 (2014).
[23]C. Freysoldt, J. Neugebauer, and C. G. V. de Walle, Phys. Rev. Lett. **102**, 016402 (2009).
[24]Y. Kumagai and F. Oba, Phys. Rev. B **89**, 195205 (2014).
[25]T. Gake, Y. Kumagai, C. Freysoldt, and F. Oba, Phys. Rev. B **101**, 020102 (2020).
[26]J. Sun, A. Ruzsinszky, and J. Perdew, Phys. Rev. Lett. **115**, 036402 (2015).
[27]A. Tiede, "Investigations on electron accumulation at $\kappa$-$Ga_2O_3$-$\kappa$-$(AlGa)_2O_3$ heterointerfaces," Master's thesis (University of Leipzig, 2021).
[28]D. Splith, S. Müller, H. Wenckstern, and M. Grundmann, Phys. Status Solidi A **218**, 2100121 (2021).
[29]M. E. Ingebrigtsen, A. Y. Kuznetsov, B. G. Svensson, G. Alfieri, A. Mihaila, U. Badstübner, A. Perron, L. Vines, and J. B. Varley, APL Mater. **7**, 022510 (2019).
[30]Y. K. Frodason, C. Zimmermann, E. F. Verhoeven, P. M. Weiser, L. Vines, and J. B. Varley, Phys. Rev. Mater. **5**, 025402 (2021).
[31]Y. K. Frodason, J. B. Varley, K. M. H. Johansen, L. Vines, and C. G. V. de Walle, Phys. Rev. B **107**, 024109 (2023).
[32]J. B. Varley, J. R. Weber, A. Janotti, and C. G. Van de Walle, Appl. Phys. Lett. **97**, 142106 (2010).
[33]J. B. Varley, H. Peelaers, A. Janotti, and C. G. V. de Walle, J. Phys.: Condens Matter **23**, 334212 (2011).
[34]S. Lany, APL Mater. **6**, 046103 (2018).
[35]J. B. Varley, A. Perron, V. Lordi, D. Wickramaratne, and J. L. Lyons, Appl. Phys. Lett. **116**, 172104 (2020).
[36]M. Wang, S. Mu, and C. G. V. de Walle, J. Appl. Phys. **130**, 185703 (2021).
[37]M. E. Ingebrigtsen, J. B. Varley, A. Y. Kuznetsov, B. G. Svensson, G. Alfieri, A. Mihaila, U. Badstübner, and L. Vines, Appl. Phys. Lett. **112**, 042104 (2018).
[38]C. Zimmermann, Y. K. Frodason, A. W. Barnard, J. B. Varley, K. Irmscher, Z. Galazka, A. Karjalainen, W. E. Meyer, F. D. Auret, and L. Vines, Appl. Phys. Lett. **116**, 072101 (2020).
[39]J. F. McGlone, Z. Xia, C. Joishi, S. Lodha, S. Rajan, S. Ringel, and A. R. Arehart, Appl. Phys. Lett. **115**, 153501 (2019).
[40]K. Irmscher, Z. Galazka, M. Pietsch, R. Uecker, and R. Fornari, J. Appl. Phys. **110**, 063720 (2011).
[41]A. Polyakov, N. Smirnov, I. Shchemerov, D. Gogova, S. Tarelkin, and S. Pearton, J. Appl. Phys. **123**, 115702 (2018).
[42]B. Wang, D. Look, and K. Leedy, J. Appl. Phys. **125**, 105103 (2019).
[43]M. Kneiß, A. Hassa, D. Splith, C. Sturm, H. von Wenckstern, T. Schultz, N. Koch, M. Lorenz, and M. Grundmann, APL Mater. **7**, 022516 (2019).
[44]Y. Zhuo, Z. Chen, W. Tu, X. Ma, Y. Pei, and G. Wang, Appl. Surf. Sci. **420**, 802 (2017).
[45]D. Tahara, H. Nishinaka, S. Morimoto, and M. Yoshimoto, Appl. Phys. Lett. **112**, 152102 (2018).
[46]H. Nishinaka, D. Tahara, and M. Yoshimoto, Jpn. J. Appl. Phys. **55**, 1202BC (2016).
[47]M. Mulazzi, F. Reichmann, A. Becker, W. Klesse, P. Alippi, V. Fiorentini, A. Parisini, M. Bosi, and R. Fornari, APL Mater. **7**, 022522 (2019).

20 February 2024 10:56:07



Published under an exclusive license by AIP Publishing